Journal of Alloys and Compounds 480 (2009) 756–760

Contents lists available at ScienceDirect

Journal of Alloys and Compounds

journal homepage: www.elsevier.com/locate/jallcom

# Structural investigation and electrochemical properties of $La_{5-x}Ca_xMg_2Ni_{23}$ ($x = 0$, 1, 2 and 3) hydrogen storage alloys

T.Z. Si[a,b], G. Pang[a], D.M. Liu[a], Q.A. Zhang[a,*], N. Liu[b]

[a] School of Materials Science and Engineering, Anhui University of Technology, Maanshan, Anhui 243002, PR China
[b] School of Materials Science and Engineering, Hefei University of Technology, Hefei, Anhui 230009, PR China

ARTICLE INFO

*Article history:*
Received 2 January 2009
Received in revised form 9 February 2009
Accepted 10 February 2009
Available online 23 February 2009

*Keywords:*
$La_5Mg_2Ni_{23}$ alloy
Ca substitution
Phase structure
Electrochemical property

ABSTRACT

The structures and electrochemical properties of the $La_{5-x}Ca_xMg_2Ni_{23}$ ($x = 0$, 1, 2 and 3) alloys were investigated. It was found that the $La_5Mg_2Ni_{23}$ alloy consists of $Ce_2Ni_7$-type, $Gd_2Co_7$-type, $LaNi_5$, $Pr_5Co_{19}$-type, $Ce_5Co_{19}$-type and $LaMgNi_4$ phases. Ca substitution for La is favorable for the formation of the $PuNi_3$-type phase. The Ca-substituted $La_{5-x}Ca_xMg_2Ni_{23}$ alloys are composed of $PuNi_3$-type, $Gd_2Co_7$-type and $CaCu_5$-type phases, except for the $La_2Ca_3Mg_2Ni_{23}$ alloy additionally containing 4 wt.% of Ni. Among these alloys, the $La_3Ca_2Mg_2Ni_{23}$ alloy has a highest discharge capacity (404.2 mAh/g) and a best high-rate dischargeability ($HRD_{600} = 61.6\%$) due to the optimum Ca content and the highest abundance of the $PuNi_3$-type and $Gd_2Co_7$-type phases.



## 1. Introduction

In the last decade, the La–Mg–Ni-based alloys with superlattice structures have attracted extensive attention due to their good electrochemical properties [1–5]. The unit cells of these alloys are made of $A_2B_4$ (Laves)-type and $AB_5$-type units stacking along the crystallographic *c*-axis [6]. For example, each block of the $PuNi_3$-type $La_2MgNi_9$ unit cell consists of one $A_2B_4$ unit ($LaMgNi_4$) and one $AB_5$ ($LaNi_5$) unit, while that of $La_3MgNi_{14}$ unit cell ($Ce_2Ni_7$-type structure) is composed of one $A_2B_4$ ($LaMgNi_4$) and two $AB_5$ ($LaNi_5$) units. Recently, Kohno et al. reported that the $La_5Mg_2Ni_{23}$ ($La_{0.7}Mg_{0.3}Ni_{2.8}Co_{0.5}$) alloy possessed a maximum discharge capacity of 410 mAh/g, which is 1.3 times as large as that of $LaNi_5$ [7]. They believed that the $La_5Mg_2Ni_{23}$ alloy was present as a single phase with an unit cell containing a long-range stacking arrangement of $LaNi_3$ and $La_2Ni_7$. Differentiating from $La_2MgNi_9$ and $La_3MgNi_{14}$, each block of $La_5Mg_2Ni_{23}$ unit cell was assumed to be composed of two $A_2B_4$ units and three $AB_5$ units. However, the $La_5Mg_2Ni_{23}$ structure has not been confirmed up to now. In the present work, therefore, the $La_5Mg_2Ni_{23}$ alloy has been prepared at first for an attempt to obtain the $La_5Mg_2Ni_{23}$ phase. Unfortunately, the $La_5Mg_2Ni_{23}$ phase has not been found under the present condition.

Similar to La–Mg–Ni compounds, the Ca–Mg–Ni compounds also have superlattice structures, in which [$CaNi_5$] units and [$CaMgNi_4$] units stack along the *c*-axis according to certain combinations [8,9]. Recently, we found a new ternary intermetallic compound $Ca_3Mg_2Ni_{13}$ crystallizing in space group $R\bar{3}m$ [9]. It is noteworthy that each block in $Ca_3Mg_2Ni_{13}$ structure contains two $A_2B_4$ ($CaMgNi_4$) units and one $AB_5$ ($CaNi_5$) unit. However, the corresponding $La_3Mg_2Ni_{13}$ compound has not been found in the La–Mg–Ni system. This means that the difference of atomic radius between Ca and La might affect the phase stability. Thus it is necessary to understand whether the $La_5Mg_2Ni_{23}$ phase forms by means of partial substitution of La by Ca.

On the other hand, the Ca-substituted $PuNi_3$-type La–Mg–Ni alloys possessed higher hydrogen storage capacities due to the light weight of Ca element [10,11]. Moreover, the discharge kinetics for the La–Mg–Ni alloys can be improved by the substitution [12]. In this paper, the $La_{5-x}Ca_xMg_2Ni_{23}$ ($x = 0$, 1, 2 and 3) alloys were prepared to investigate the effect of Ca substitution on the structures and electrochemical properties.

### 2. Experimental details

The $La_{5-x}Ca_xMg_2Ni_{23}$ ($x = 0$, 1, 2 and 3) alloys were prepared by induction melting of appropriate amounts of pure metals under Ar atmosphere (0.06 MPa). The losses of La, Ca and Mg were determined to be about 2, 10 and 16 wt.% by repetitious experiments, respectively. On the basis of stoichiometric amounts of starting materials, thus, extra 2 wt.% of La, 10 wt.% of Ca and 16 wt.% of Mg were added to compensate the losses of La, Ca and Mg during melting. The alloys were remelted three times to ensure homogeneity. After remelting, the alloys were annealed at 723 K for 2 days and subsequently 1023 K for 3 days under Ar atmosphere.

All alloys were crushed mechanically into powders of 300 mesh under Ar atmosphere. XRD measurements were carried out using a Rigaku D/Max 2500VL/PC diffractometer with Cu Kα radiation at 50 kV and 150 mA. The XRD profiles were analyzed with the Rietveld refinement program RIETAN-2000 [13]. The microstructures of the $La_{5-x}Ca_xMg_2Ni_{23}$ ($x = 0$, 1, 2 and 3) alloys were examined using a scanning

* Corresponding author. Tel.: +86 555 2311570; fax: +86 555 2471263.
*E-mail address:* zhang03jp@yahoo.com.cn (Q.A. Zhang).

0925-8388/$ – see front matter © 2009 Elsevier B.V. All rights reserved.
doi:10.1016/j.jallcom.2009.02.038

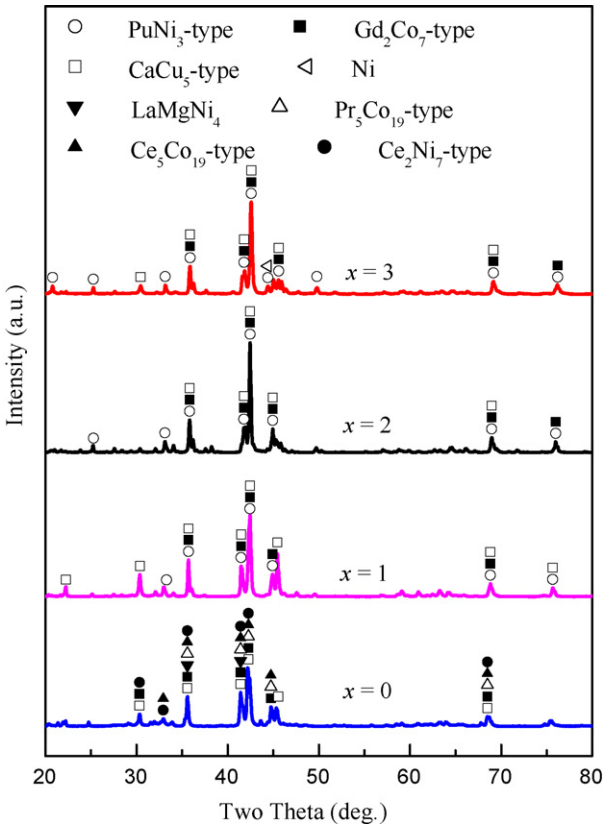


**Fig. 1.** XRD patterns of the $La_{5-x}Ca_xMg_2Ni_{23}$ ($x = 0$, 1, 2 and 3) alloys.

electron microscope (SEM) XL30 with an energy-dispersive X-ray spectrometer (EDS) at an accelerating voltage of 20 kV.

The test electrodes were prepared by cold pressing the alloy powders with copper powder in a weight ratio of 1:2 into pellets with Ø10 mm × 2 mm. Electrochemical charge–discharge tests were carried out at 298 K by using a Land battery testing system. The positive counter electrode and reference electrode were $Ni(OH)_2$/NiOOH and Hg/HgO, respectively. The test electrodes were charged at 100 mA/g for 6 h and discharged at 50 mA/g to the cut-off potential of −0.6 V versus Hg/HgO reference electrode. High-rate dischargeability (HRD) was determined from a ratio of the discharge capacity at a given discharge current density (100–600 mA/g) to the discharge capacity at 50 mA/g. In order to investigate the corrosion behavior of the $La_{5-x}Ca_xMg_2Ni_{23}$ ($x = 0$, 1, 2 and 3) alloys, polarization curves were measured using the CHI 660b electrochemical workstation at a scan rate of 1 mV/s within the potential interval of −1.2 to −0.6 V versus Hg/HgO.

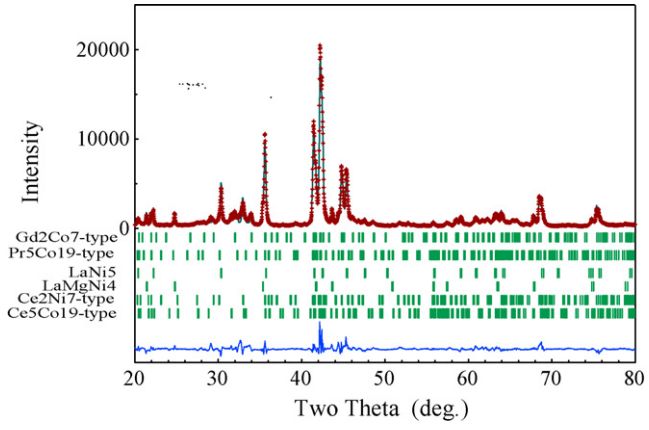


**Fig. 2.** Calculated (line) and observed (+) X-ray diffraction patterns for the $La_5Mg_2Ni_{23}$ alloy. The difference between the observed and calculated patters is shown as the bottom solid line.

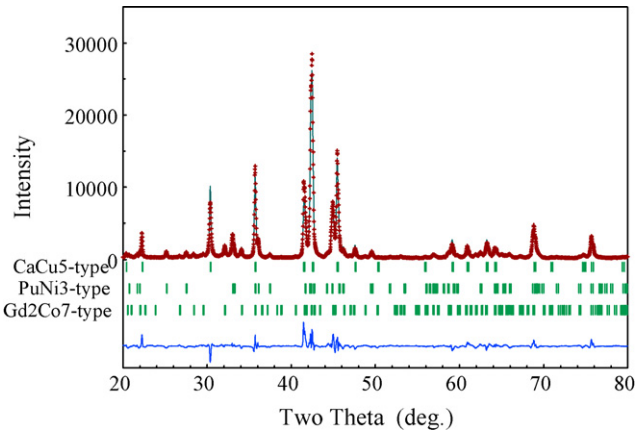


**Fig. 3.** Calculated (line) and observed (+) X-ray diffraction patterns for the $La_4CaMg_2Ni_{23}$ alloy. The difference between the observed and calculated patters is shown as the bottom solid line.

## 3. Results and discussion

### 3.1. Phase structures

Fig. 1 shows the XRD patterns of the $La_{5-x}Ca_xMg_2Ni_{23}$ ($x = 0$, 1, 2 and 3) alloys. It can be seen that all the alloys consist of multiple phases. It is generally accepted that the La–Mg–Ni ternary alloys prepared by induction melting have multi-phase microstructures due to nonequilibrium solidification [14–18]. Differentiating from the result reported in Ref. [7], the $La_5Mg_2Ni_{23}$ alloy consists of $Ce_2Ni_7$-type, $Gd_2Co_7$-type, $LaNi_5$, $Pr_5Co_{19}$-type, $Ce_5Co_{19}$-type and $LaMgNi_4$ phases. The Rietveld analysis result for the $La_5Mg_2Ni_{23}$ alloy is shown in Fig. 2. For the Rietveld refinement, the structure models for the above six phases were, respectively, taken from the reported structures for $Ce_2Ni_7$, $Gd_2Co_7$ [19], $Pr_5Co_{19}$-type, $Ce_5Co_{19}$-type [20], $CaCu_5$ [21] and $MgCu_4Sn$ [22]. As shown in Fig. 2, the diffraction pattern calculated from the structure models is in good agreement with that measured.

The Ca-substituted $La_5Mg_2Ni_{23}$ alloys are composed of $PuNi_3$-type, $Gd_2Co_7$-type and $CaCu_5$-type phases, except for the $La_2Ca_3Mg_2Ni_{23}$ alloy additionally containing 4 wt.% of Ni. The Rietveld analysis result for the $La_4CaMg_2Ni_{23}$ alloy is shown in Fig. 3 as a representative example of the $La_{5-x}Ca_xMg_2Ni_{23}$ ($x = 1$, 2 and 3) alloys. The structural parameters and phase abundance of the $La_{5-x}Ca_xMg_2Ni_{23}$ alloys refined by the XRD Rietveld analysis are listed in Table 1. It can be seen that the Ca substitution

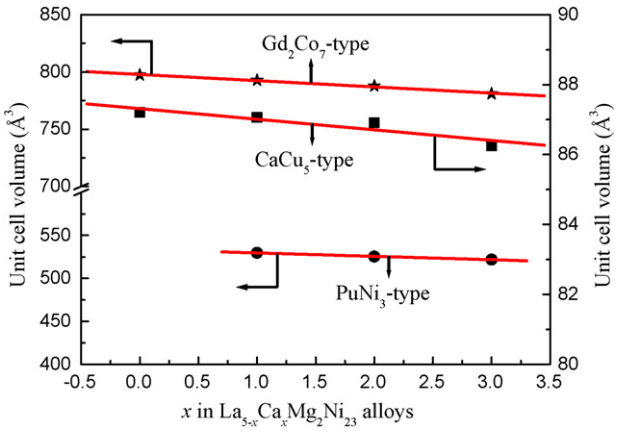


**Fig. 4.** Relations of unit cell volumes of the $Gd_2Co_7$-type, $CaCu_5$-type and $PuNi_3$-type phases with Ca content in the $La_{5-x}Ca_xMg_2Ni_{23}$ alloys.

**Table 1**
Structural parameters and phase abundance of the $La_{5-x}Ca_xMg_2Ni_{23}$ ($x$ = 0, 1, 2 and 3) alloys refined by the X-ray Rietveld analysis.

| Alloy | Phase | Space group | $R_I$ (%) | Lattice parameters (Å) | | Abundance (wt.%) |
|---|---|---|---|---|---|---|
| | | | | $a$ | $c$ | |
| $La_5Mg_2Ni_{23}$ $R_{wp}$ = 14.86% $S$ = 3.34 | $Ce_2Ni_7$-type | $P6/mmm$ | 3.36 | 5.0399(4) | 24.251(7) | 21 |
| | $Gd_2Co_7$-type | $R\bar{3}m$ | 3.18 | 5.0317(3) | 36.363(2) | 17 |
| | $LaNi_5$ | $P6/mmm$ | 3.19 | 5.0232(3) | 3.991(0) | 25 |
| | $Ce_5Co_{19}$-type | $R\bar{3}m$ | 3.06 | 5.0295(7) | 48.334(6) | 17 |
| | $Pr_5Co_{19}$-type | $P6/mmm$ | 2.81 | 5.0386(9) | 32.260(3) | 10 |
| | $LaMgNi_4$ | $F\bar{4}3m$ | 2.63 | 7.1742(2) | | 10 |
| $La_4CaMg_2Ni_{23}$ $R_{wp}$ = 11.83% $S$ = 2.81 | $PuNi_3$-type | $R\bar{3}m$ | 2.50 | 5.0237(2) | 24.235(4) | 29 |
| | $Gd_2Co_7$-type | $R\bar{3}m$ | 1.92 | 5.0236(1) | 36.271(1) | 36 |
| | $CaCu_5$-type | $P6/mmm$ | 1.87 | 5.0222(6) | 3.985(7) | 35 |
| $La_3Ca_2Mg_2Ni_{23}$ $R_{wp}$ = 12.95% $S$ = 3.28 | $PuNi_3$-type | $R\bar{3}m$ | 3.16 | 5.0081(6) | 24.183(2) | 51 |
| | $Gd_2Co_7$-type | $R\bar{3}m$ | 3.37 | 5.0028(5) | 36.343(7) | 37 |
| | $CaCu_5$-type | $P6/mmm$ | 2.13 | 5.0169(1) | 3.987(1) | 12 |
| $La_2Ca_3Mg_2Ni_{23}$ $R_{wp}$ = 10.70% $S$ = 2.78 | $PuNi_3$-type | $R\bar{3}m$ | 2.18 | 4.9970(5) | 24.130(0) | 61 |
| | $Gd_2Co_7$-type | $R\bar{3}m$ | 2.46 | 4.9939(0) | 36.155(7) | 13 |
| | $CaCu_5$-type | $P6_3/mmc$ | 2.23 | 5.0042(0) | 3.977(3) | 22 |
| | Ni | $Fm\bar{3}m$ | 2.10 | 3.5304(1) | | 4 |

is favorable for the formation of the $PuNi_3$-type phase. Its phase abundance increases from 29 to 61 wt.% with increasing Ca content from $x$ = 1 to 3. It is interesting that the $Ce_2Ni_7$-type phase entirely disappears in the Ca-substituted $La_5Mg_2Ni_{23}$ alloys. It was reported that the $A_2B_7$-type La–Mg–Ni phase has $Ce_2Ni_7$-type or $Gd_2Co_7$-type structure [19], while the $A_2B_7$-type Ca–Mg–Ni phase has only the $Gd_2Co_7$-type structure [9]. Therefore, the Ca-substituted $Ce_2Ni_7$-type phase is unstable and transforms into the $Gd_2Co_7$-type phase in the $La_{5-x}Ca_xMg_2Ni_{23}$ ($x$ = 1, 2 and 3) alloys. Moreover, the addition of Ca is also unbeneficial for the formation of the $Pr_5Co_{19}$-type, $Ce_5Co_{19}$-type and $LaMgNi_4$ phases. Therefore, the Ca-substituted $La_5Mg_2Ni_{23}$ alloys consist of the $Gd_2Co_7$-type, $CaCu_5$-type and $PuNi_3$-type phases. The cell volumes of these phases decrease linearly with increasing Ca content (as shown in Fig. 4) because the atom radius of Ca is smaller than that of La.

The back-scattered SEM images of the $La_{5-x}Ca_xMg_2Ni_{23}$ ($x$ = 0, 1, 2 and 3) alloys are shown in Fig. 5. The phases were distinguished by energy-dispersive spectroscope (EDS) measurements. The arrows A, B, C and E indicate $A_2B_7$-type, $LaNi_5$, $LaMgNi_4$, and $A_5B_{19}$-type phases in Fig. 5a, respectively. Owing to the same composition of the $Ce_2Ni_7$-type and $Gd_2Co_7$-type phases, they cannot be

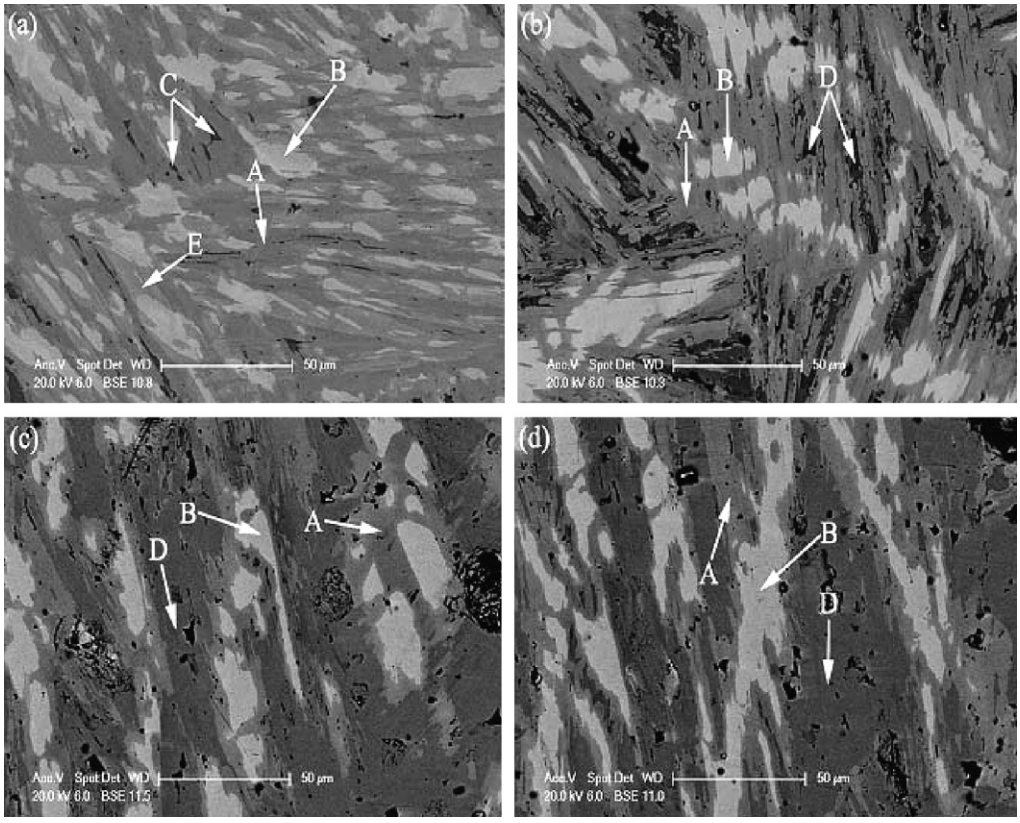


**Fig. 5.** Back-scattered SEM images of the $La_{5-x}Ca_xMg_2Ni_{23}$ ($x$ = 0, 1, 2 and 3) alloys.

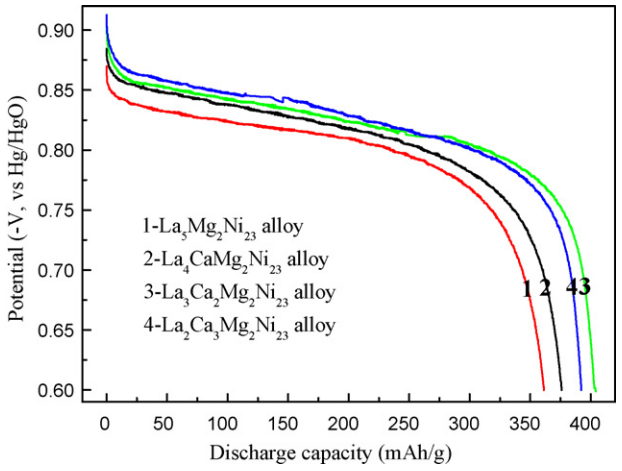


**Fig. 6.** Discharge curves of the $La_{5-x}Ca_xMg_2Ni_{23}$ ($x = 0$, 1, 2 and 3) alloys.

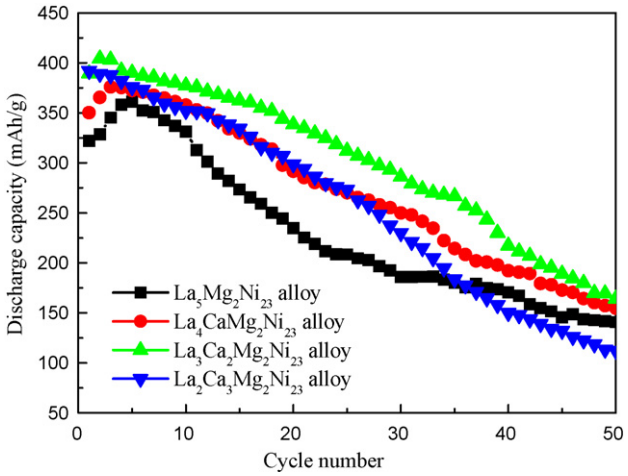


**Fig. 7.** Discharge capacity versus cycle number for the $La_{5-x}Ca_xMg_2Ni_{23}$ ($x = 0$, 1, 2 and 3) alloys (charged at 100 mA/g for 6 h, discharged to −0.6 V at 50 mA/g).

distinguished in the SEM image. Similar condition also occurred for the $Pr_5Co_{19}$-type and $Ce_5Co_{19}$-type phases. The arrows A, B and D indicate $Gd_2Co_7$-type, $CaCu_5$-type, and $PuNi_3$-type phases in Fig. 5b–d, respectively. These results of back-scattered SEM are consistent with the XRD Rietveld analysis results.

### 3.2. Electrochemical properties

Fig. 6 shows the discharge curves of the $La_{5-x}Ca_xMg_2Ni_{23}$ ($x = 0$, 1, 2 and 3) alloy electrodes. The discharge plateaus shift toward a more negative potential with increasing Ca content in the alloys. It is reasonable that the high discharge plateau is attributed to the small cell volumes of the phases in the Ca-substituted $La_5Mg_2Ni_{23}$ alloys.

The maximum discharge capacities are summarized in Table 2. With increasing Ca content from $x = 0$ to 2, the maximum discharge capacity increases from 361.2 to 404.2 mAh/g. However, the maximum discharge capacity decreases to 392.2 mAh/g when $x = 3$. This result might be caused by the following two factors. One is that the lighter weight of Ca would result in the higher hydrogen storage capacity. The other is related to the phase components of the $La_{5-x}Ca_xMg_2Ni_{23}$ alloys. It was reported that the $A_2B_7$-type La–Mg–Ni phase has a discharge capacity of 380 mAh/g [19], and the discharge capacity of the $PuNi_3$-type phase is comparable with that of the $A_2B_7$-type phase [7]. However, the $LaMgNi_4$ phase has only a discharge capacity of 300 mAh/g [23], which is close to that of $LaNi_5$. Therefore, the phase abundance influences the discharge capacities of the $La_{5-x}Ca_xMg_2Ni_{23}$ alloys.

Fig. 7 shows the discharge capacity versus charging–discharging cycle number for the $La_{5-x}Ca_xMg_2Ni_{23}$ alloys. It can be seen that the alloy electrodes can be easily activated to their maximum discharge capacity within four cycles. The cycling capacity retention rates of the alloys after 50 cycles, expressed as $S_{50} = C_{50}/C_{max} \times 100\%$ (where $C_{max}$ is the maximum discharge capacity, and $C_{50}$ is the discharge capacity at the 50th cycle), are 39%, 41.1%, 40.6% and 28.6%, respectively. As reported previously, the $PuNi_3$-type and $Gd_2Co_7$-type phases have better cyclic stabilities than the $LaNi_5$ and $LaMgNi_4$ phases [24,25]. Moreover, the cyclic stability of the $Gd_2Co_7$-type phase is superior to that of the $PuNi_3$-type phase [26]. Though higher Ca content leads to a poor corrosion resistance, the cyclic stabilities of the $La_4CaMg_2Ni_{23}$ and $La_3Ca_2Mg_2Ni_{23}$ alloys does not decrease due to the increase in the amount of the $PuNi_3$-type and $Gd_2Co_7$-type phases. The polarization curves of the alloys are present in Fig. 8. It can be seen that the corrosion potential $E_{corr}$ reduces with increasing Ca content in the $La_{5-x}Ca_xMg_2Ni_{23}$ alloys. Especially, the $E_{corr}$ value of the $La_2Ca_3Mg_2Ni_{23}$ alloy decreases to −1.008 V. This suggests that the cycling capacity retention rates of the $La_{5-x}Ca_xMg_2Ni_{23}$ alloys are related to both phase abundance and corrosion potential.

In order to investigate the high-rate dischargeability (HRD) of the $La_{5-x}Ca_xMg_2Ni_{23}$ alloys, the effect of the discharge current density (50–600 mA/g) on the discharge capacity is shown in Fig. 9. It is generally accepted that the HRD of MH electrode is influenced mainly by the electrochemical reaction kinetics on the alloy powder surface and the diffusion rate of hydrogen [27–29]. The Ca substitution for La results in the acceleration of dehydriding process due to the lower stability of metal hydride. Moreover, the high abundance of $PuNi_3$-type and $Gd_2Co_7$-type phases with good HRD also has a contribution to the HRD of the $La_4CaMg_2Ni_{23}$ and $La_3Ca_2Mg_2Ni_{23}$ alloys. Therefore, the $HRD_{600}$ increases from 54% ($x = 0$) to 58% ($x = 1$) and 61.6% ($x = 2$), respectively. However, the

**Table 2**
Electrochemical properties of the $La_{5-x}Ca_xMg_2Ni_{23}$ ($x = 0$, 1, 2 and 3) alloy electrodes ($N^a$: the activation number).

| Alloy | $C_{max}$ (mAh/g) | $N^a$ | $S_{50}$ (%) | $HRD_{600}$ (%) | $E_{corr}$ (V) |
|---|---|---|---|---|---|
| $La_5Mg_2Ni_{23}$ | 361.2 | 5 | 39 | 54 | −0.939 |
| $La_4CaMg_2Ni_{23}$ | 376 | 3 | 41.1 | 58 | −0.951 |
| $La_3Ca_2Mg_2Ni_{23}$ | 404.2 | 2 | 40.6 | 61.6 | −0.961 |
| $La_2Ca_3Mg_2Ni_{23}$ | 392.2 | 1 | 28.6 | 44 | −1.008 |

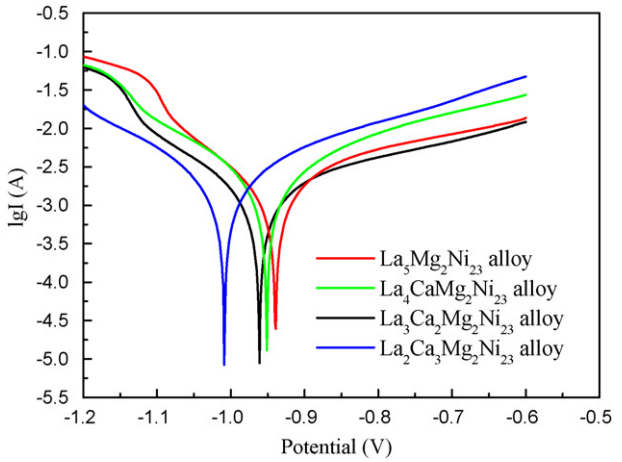


**Fig. 8.** Polarization curves of the $La_{5-x}Ca_xMg_2Ni_{23}$ ($x = 0$, 1, 2 and 3) alloys.

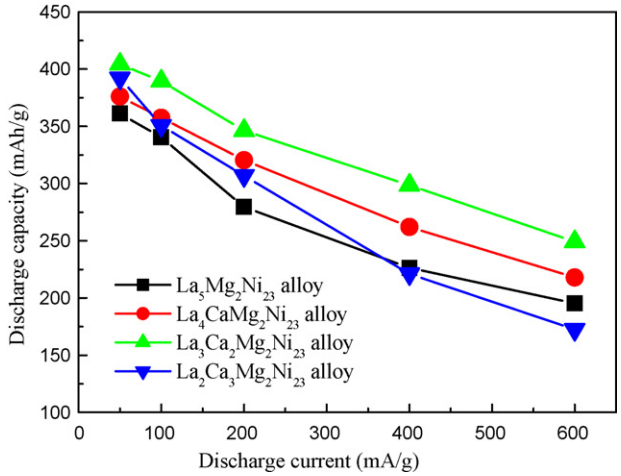


**Fig. 9.** Discharge capacities of the $La_{5-x}Ca_xMg_2Ni_{23}$ ($x$ = 0, 1, 2 and 3) alloys at different discharge current densities.

corrosion products increase the charge transfer resistance during discharging on the alloy surface, and therefore the surface reaction kinetics is decreased. Due to the poor corrosion resistance of the $La_2Ca_3Mg_2Ni_{23}$ alloy, this alloy has a lowest HRD ($HRD_{600}$ = 44%).

## 4. Conclusions

The effect of the Ca substitution for La on the structures and electrochemical properties of the $La_{5-x}Ca_xMg_2Ni_{23}$ ($x$ = 0, 1, 2 and 3) alloys was investigated. It was found that the $La_5Mg_2Ni_{23}$ alloy consists of $Ce_2Ni_7$-type, $Gd_2Co_7$-type, $LaNi_5$, $Pr_5Co_{19}$-type, $Ce_5Co_{19}$-type and $LaMgNi_4$ phases. Ca substitution is favorable for the formation of the $PuNi_3$-type phase. The $La_{5-x}Ca_xMg_2Ni_{23}$ ($x$ = 1, 2 and 3) alloys are composed of $PuNi_3$-type, $Gd_2Co_7$-type and $CaCu_5$-type phases (4 wt.% Ni additionally appeared in the $La_2Ca_3Mg_2Ni_{23}$ alloy). The $La_{5-x}Ca_xMg_2Ni_{23}$ ($x$ = 0, 1, 2 and 3) alloys can be activated to their maximum discharge capacities within four cycles. The cyclic stabilities of the $La_{5-x}Ca_xMg_2Ni_{23}$ alloys are related to both phase abundance and corrosion potential. The discharge capacities of the Ca-substituted alloys are higher than that of the $La_5Mg_2Ni_{23}$ alloy. Among these alloys, the $La_3Ca_2Mg_2Ni_{23}$ alloy has a highest discharge capacity (404.2 mAh/g) and a best high-rate dischargeability ($HRD_{600}$ = 61.6%) due to the optimum Ca content and the highest abundance of the $PuNi_3$-type and $Gd_2Co_7$-type phases.

## Acknowledgements

This work is supported by the National Natural Science Foundation of China (No. 50771001), the Natural Science Foundation of Anhui Province (No. 070414159) and the Scientific Research Foundation of Education Department of Anhui Province of China (No. KJ2008A149).

## References

[1] Y.F. Liu, H.G. Pan, M.X. Gao, Y.F. Zhu, H.W. Ge, S.Q. Li, Y.Q. Lei, Acta Metall. Sin. 39 (2003) 666–672.
[2] H.G. Pan, Y.F. Liu, M.X. Gao, Y.Q. Lei, Q.D. Wang, J. Electrochem. Soc. 152 (2005) A326–A332.
[3] H.G. Pan, Q.W. Jin, M.X. Gao, Y.F. Liu, R. Li, Y.Q. Lei, J. Alloys Compd. 373 (2004) 237–245.
[4] H.G. Pan, Y.F. Liu, M.X. Gao, Y.F. Zhu, Y.Q. Lei, Int. J. Hydrogen Energy 28 (2003) 1219–1228.
[5] T.Z. Si, Q.A. Zhang, N. Liu, Int. J. Hydrogen Energy 33 (2008) 1729–1734.
[6] E. Akiba, H. Hayakawa, T. Kohno, J. Alloys Compd. 408–412 (2006) 280–283.
[7] T. Kohno, H. Yoshida, F. Kawashima, T. Inaba, I. Sakai, M. Yamamoto, M. Kanda, J. Alloys Compd. 311 (2000) L5–L7.
[8] K. Kadir, N. Kuriyama, T. Sakai, I. Uehara, L. Eriksson, J. Alloys Compd. 284 (1999) 145–154.
[9] Q.A. Zhang, G. Pang, T.Z. Si, D.M. Liu, Acta Mater. (2009), doi:10.1016/j.actamat.2008.12.040.
[10] K. Kadir, T. Sakai, I. Uehara, J. Alloys Compd. 302 (2000) 112–117.
[11] J. Chen, N. Kuriyama, H.T. Takeshita, H. Tanaka, T. Sakai, M. Haruta, Electrochem. Solid-State Lett. 396 (2000) 249–258.
[12] P. Zhang, Y.F. Liu, R. Tang, J.W. Zhu, X.D. Wei, S.S. Liu, G. Yu, Electrochim. Acta 51 (2006) 6400–6405.
[13] F. Izumi, T. Ikeda, Mater. Sci. Forum 321–323 (2000) 198–203.
[14] Y.F. Liu, H.G. Pan, M.X. Gao, R. Li, Y.Q. Lei, J. Alloys Compd. 376 (2004) 304–313.
[15] Y.F. Liu, H.G. Pan, Y.J. Yue, X.F. Wu, N. Chen, Y.Q. Lei, J. Alloys Compd. 395 (2005) 291–299.
[16] H.G. Pan, Y.J. Yue, M.X. Gao, X.F. Wu, N. Chen, Y.Q. Lei, Q.D. Wang, J. Alloys Compd. 397 (2005) 269–275.
[17] Y.F. Liu, H.G. Pan, M.X. Gao, R. Li, Y.Q. Lei, J. Alloys Compd. 389 (2005) 281–289.
[18] S. Ma, M.X. Gao, R. Li, H.G. Pan, Y.Q. Lei, J. Alloys Compd. 457 (2008) 457–464.
[19] F.L. Zhang, Y.C. Luo, J.P. Chen, R.X. Yan, J.H. Chen, J. Alloys Compd. 430 (2007) 302–307.
[20] H. Hayakawa, E. Akiba, M. Gotoh, T. Kohno, Mater. Trans. 46 (2005) 1393–1401.
[21] R.H. Wiswall, J.J. Reily, Inorg. Chem. 11 (1972) 1691–1698.
[22] L. Guenee, V. Favre-Nicolin, K. Yvon, J. Alloys Compd. 348 (2003) 129–137.
[23] Z.M. Wang, H.Y. Zhou, Z.F. Gu, G. Cheng, A.B. Yu, J. Alloys Compd. 377 (2004) L7–L9.
[24] B. Liao, Y.Q. Lei, G.L. Lu, L.X. Chen, H.G. Pan, Q.D. Wang, J. Alloys Compd. 356/357 (2003) 746–749.
[25] K.H.J. Buschow, in: K.A. Gschneidner Jr., L. Eyring (Eds.), Handbook on the Physics and Chemistry of Rare Earths, Elsevier, Amsterdam, 1984, p. 1.
[26] F.L. Zhang, Y.C. Luo, J.P. Chen, R.X. Yan, L. Kang, J.H. Chen, J. Power Sources 150 (2005) 247–254.
[27] H.G. Pan, J.X. Ma, C.S. Wang, S.A. Chen, X.H. Wang, C.P. Chen, Q.D. Wang, J. Alloys Compd. 293–295 (1999) 648–652.
[28] Y.F. Zhu, H.G. Pan, M.X. Gao, J.X. Ma, S.Q. Li, Q.D. Wang, Int. J. Hydrogen Energy 27 (2002) 287–293.
[29] H.G. Pan, Y.F. Zhu, M.X. Gao, Y.F. Liu, R. Li, Y.Q. Lei, Q.D. Wang, J. Alloys Compd. 370 (2004) 254–260.